Kobe University Repository : Kernel

PDF issue: 2026-05-19

Carbon dioxide reduction to methanol with water using visible light-activated organic photocatalysts selected based on DFT calculations

Ichihashi, Yuichi
Shishida, Kazuki
Oishi, Kaito
Nishikawa, Daisuke

(Citation)
Catalysis Today,461:115530

(Issue Date)
2026-01-01

(Resource Type)
journal article

(Version)
Version of Record

(Rights)
© 2025 The Author(s). Published by Elsevier B.V.
This is an open access article under the Creative Commons Attribution 4.0 International license

(URL)
https://hdl.handle.net/20.500.14094/0100497594

Catalysis Today 461 (2026) 115530

Contents lists available at ScienceDirect

Catalysis Today

journal homepage: www.elsevier.com/locate/cattod

Carbon dioxide reduction to methanol with water using visible light-activated organic photocatalysts selected based on DFT calculations

Yuichi Ichihashi [a,b,*], Kazuki Shishida [a], Kaito Oishi [a], Daisuke Nishikawa [c]

[a] Department of Applied Chemistry, Graduate School of Engineering, Kobe University, Rokkodai, Nada, Kobe 657-8501, Japan
[b] Research Center for Membrane and Film Technology, Kobe University, Rokkodai, Nada, Kobe 657-8501, Japan
[c] The Center for Environmental Conservation, Kobe University, Rokkodai, Nada, Kobe 657-8501, Japan

ARTICLE INFO

Keywords:
Photocatalytic reduction of carbon dioxide
Organic photocatalyst
Visible light irradiation
Polycyclic aromatic compounds

ABSTRACT

Photocatalytic reduction of CO_2 is a viable approach to achieve carbon neutrality. In this study, density functional theory (DFT) calculations predicted that polycyclic aromatic hydrocarbons, picene, 5,8-dicyanopicene (CN-picene), 2,7-dicyanopyrene (CN-pyrene), and 9,10-dicyanoanthracene (CN-anthracene), as photocatalysts for CO_2 reduction driven by UV or visible light exposure. Notably, CN-anthracene was predicted to be the most effective photocatalyst under visible light irradiation. Therefore, photocatalytic performance of CN-anthracene in converting CO_2 into methanol by visible light exposure in an aqueous medium was examined. Methanol production was observed upon irradiation CN-anthracene with visible light, involving CO_2 and H_2O. Reusability experiments showed that CN-anthracene can facilitate stable methanol production even after three cycles of photocatalytic activity. Photocatalytic reduction of CO_2 performed using D_2O, instead of H_2O, confirmed that the produced methanol results from water, without involving the decomposition of the photocatalyst. In conclusion, CN-anthracene demonstrates high efficiency and stability as a photocatalyst for CO_2 reduction under visible light irradiation.

1. Introduction

Carbon dioxide (CO_2) is a major greenhouse gas that adversely affects the global environment. Achieving carbon neutrality—reducing net CO_2 emissions to zero by 2050—is being promoted worldwide [1,2]. Among various CO_2 conversion technologies being explored to reach this goal, photocatalytic CO_2 reduction using clean and abundant solar energy has attracted significant attention [3-6].

Numerous inorganic photocatalysts, including TiO_2 have been reported as effective for CO_2 reduction [7-11]. Photocatalysts are materials that harness light energy to drive chemical reactions and are typically composed of semiconductors. The energy difference (bandgap) between the valence band (VB) and conduction band (CB) in semiconductors enables light absorption and subsequent electron excitation. This property makes them well-suited for reactions such as CO_2 reduction. In photocatalytic CO_2 reduction, light irradiation excites electrons from the VB to the CB, generating holes (h^+) in the VB and excited electrons (e^-) in the CB. These charge carriers enable water oxidation in the VB by h^+ and CO_2 reduction in the CB by e^-. These reactions are represented by Eqs. 1 and 2:

$$2H_2O \rightarrow O_2 + 4H^+ + 4e^- \quad (1)$$

$$CO_2 + 6e^- + 6H^+ \rightarrow CH_3OH + H_2O \quad (2)$$

Efficient photocatalysis requires the suppression of electron–hole recombination by spatially separating the carriers, thereby driving the reactions described in Eqs.1 and 2. In Eq. 2, the e^- facilitates the reduction of CO_2, producing compounds such as CH_3OH [12,13].

Many inorganic photocatalysts face limitations in tuning the energy levels of their VB and CB. Their wide bandgaps often restrict activation to ultraviolet (UV) light [14-16]. In contrast, organic semiconductor photocatalysts [17-19] possess a highest occupied molecular orbital (HOMO) and a lowest unoccupied molecular orbital (LUMO), corresponding to the VB and CB, respectively. These energy levels can be tuned by molecular design, offering a significant advantage [20]. Consequently, organic semiconductors have been widely investigated for various applications, including solar cells.

In organic photocatalytic reactions, the energy levels of the HOMO and LUMO are crucial. For CO_2 photoreduction, the HOMO level must be more positive than the oxygen evolution potential (+1.23 eV vs. NHE), and the LUMO level must be more negative than the methanol

* Corresponding author at: Department of Applied Chemistry, Graduate School of Engineering, Kobe University, Rokkodai, Nada, Kobe 657-8501, Japan.
E-mail address: ichiy@kobe-u.ac.jp (Y. Ichihashi).

https://doi.org/10.1016/j.cattod.2025.115530
Received 25 May 2025; Received in revised form 15 August 2025; Accepted 24 August 2025
Available online 26 August 2025
0920-5861/© 2025 The Author(s). Published by Elsevier B.V. This is an open access article under the CC BY license (http://creativecommons.org/licenses/by/4.0/).

Abbreviations

DFT	density functional theory
CN-picene	5,8-dicyanopicene
CN-pyrene	2,7-dicyanopyrene
CN-anthracene	9,10-dicyanoanthracene
VB	valence band
CB	conduction band
Eq	equation
UV	ultraviolet
HOMO	highest occupied molecular orbital
LUMO	lowest unoccupied molecular orbital
vs	versus
NHE	normal hydrogen electrode
DMF	N,N dimethylformamide
UV–vis	UV–visible
FT-IR	Fourier-transform infrared spectroscopy
PL	Photoluminescence.

generation potential (−0.38 eV vs. NHE). The HOMO–LUMO gap also determines the wavelength of light that can initiate photocatalysis. Therefore, reducing the HOMO–LUMO gap is essential for developing visible-light-responsive photocatalysts. The energy levels of HOMO and LUMO in organic materials are strongly influenced by their molecular structure [21] and can be estimated using quantum chemical methods such as density functional theory (DFT) calculations [22].

In our previous study, we demonstrated that polycyclic aromatic hydrocarbons, such as picene, serve as efficient photocatalysts for hydrogen generation via water splitting under UV irradiation [23]. To design visible-light-responsive photocatalysts, we performed DFT calculations on picene derivatives, indicating that introducing electron-withdrawing functional groups, such as cyano groups, can reduce the HOMO–LUMO gap [21]. In particular, we predicted that 5, 8-dicyanopicene (CN-picene) could facilitate water splitting under visible light [24]. Experimentally, we confirmed that CN-picene catalyzes water splitting under visible light irradiation. These theoretical and experimental results demonstrate that DFT is highly effective for analyzing photocatalysts' electronic structures. Accordingly, DFT can be used to predict the potential of materials for CO_2 reduction.

In this study, in addition to picene and CN-picene, we conducted DFT calculations on 2,7-dicyanopyrene (CN-pyrene) and 9,10-dicyanoanthracene (CN-anthracene), which are polycyclic aromatic compounds with electron-withdrawing cyano groups, to predict their potential for CO_2 reduction as photocatalysts under visible light irradiation.

2. Materials and methods

2.1. DFT calculation

Structural optimisation and vibrational analysis of picene, CN-picene, CN-anthracene, and CN-pyrene molecules were performed using the Gaussian 16 software suite [25]. After performing the structural optimisations, the HOMO and LUMO levels of the investigated organic photocatalysts were visualized using the GaussView program [26]. All calculations were carried out using the DFT/B3LYP method, which combines Becke's three-parameter hybrid functional with the Lee–Yang–Parr non-local correlation, employing the 6–311 G (d, p) basis set. Solvent effect was investigated using water solvent (ε=78.3553) and used the polarizable continuum model (PCM) in its integral equation formalism variant (IEFPCM).

2.2. Chemicals and materials

The organic photocatalysts, CN-anthracene and picene, were purchased from Nacalai Tesque (Kyoto, Japan) and Tokyo Chemical Industry (Tokyo, Japan), respectively. The reagents used to synthesise CN-picene and CN-pyrene, including 2,7-dibromopyrene(Br-pyrene), copper cyanide (CuCN), N,N-dimethylformamide (DMF), dichloromethane, and N-methyl-2-pyrrolidone (NMP), were purchased from Nacalai Tesque. All chemicals were used as-received.

2.2.1. Synthesis of 5,8-dicyanopicene (CN-picene)

The synthesis of CN-picene was conducted following a method described in other reports [27,28]. First, 5,8-dibromopicene (Br-picene) was synthesized from picene, followed by the conversion of Br-picene to CN-picene. A mixture of Br-picene (0.1 g) and CuCN (0.082 g) was dissolved in 10 mL DMF and refluxed under a nitrogen atmosphere at 120 °C for 24 h. Subsequently, the reaction mixture was brought to room temperature (25 °C) and diluted with 50 mL dichloromethane. The resulting solution was sequentially washed with 28 % aqueous ammonia and water, followed by dehydration using $MgSO_4$. The obtained solution was then concentrated using a rotary evaporator, yielding brown powder. The obtained brown powder was washed with ethanol, collected by suction filtration, and dried in a vacuum dryer. Finally, CN-picene was obtained by recrystallization.

2.2.2. Synthesis of 2,7-dicyanopyrene (CN-pyrene)

Br-pyrene (0.30 g) and CuCN (0.37 g) were combined in 20 mL of N-methyl-2-pyrrolidone, and the mixture was refluxed under a nitrogen atmosphere at 180℃ for 48 h. The mixture was brought to room temperature (25 ℃), and subsequently, 28 % aqueous ammonia was introduced into the mixture. The obtained precipitate was washed with water, collected by suction filtration, and dried in a vacuum dryer to obtain grey powder. Finally, CN-pyrene was obtained by recrystallization [29].

2.3. Photocatalytic methanol production

The reduction of CO_2 using organic photocatalysts was performed in a batch-type quartz reactor, irradiated with visible light. In a 7.0 mL quartz reactor, the solutions prepared using 10 mg of each photocatalyst powder and 4 mL of ion-exchanged water were placed, and CO_2 gas was bubbled through the solutions for 15 min. The reactor was sealed, and CO_2 was used to purge the gas phase. A 500 W Xe lamp (Ushio, SX-UI501XQ) coupled with 420 nm cutoff filter (HOYA, UV-42) was used for visible light irradiation. The quartz reactor was placed 5 cm away from the lamp (light source). Following irradiation, the liquid phase in the reactor was subjected to analysis by gas chromatography (GC) using a hydrogen flame ionization detector (Shimadzu GC-2010), with He serving as the carrier gas.

2.4. Characterisation

The UV–visible (UV–vis) absorption measurements of the photocatalyst powders were conducted using a UV–vis spectrophotometer (Hitachi F-7000). The functional groups of the photocatalysts were evaluated using Fourier transform infrared spectroscopy (FT-IR) on a Shimadzu IRAffinity-1S. Mass spectra of the products obtained after CO_2 reduction performed using the prepared photocatalysts were measured using quadrupole mass spectrometry (QMS) performed on a Pfeiffer Vacuum HiCube80 Eco turbopumping station, and the obtained data were analyzed using the Quadera 4.62 software.

3. Results and discussion

3.1. CO_2 reduction of picene photocatalyst under UV light

The HOMO–LUMO energy levels and gaps for picene, CN-pyrene, CN-picene, and CN-anthracene, were calculated using DFT, and the results are presented in Fig. 1 and Table 1. Previous studies have

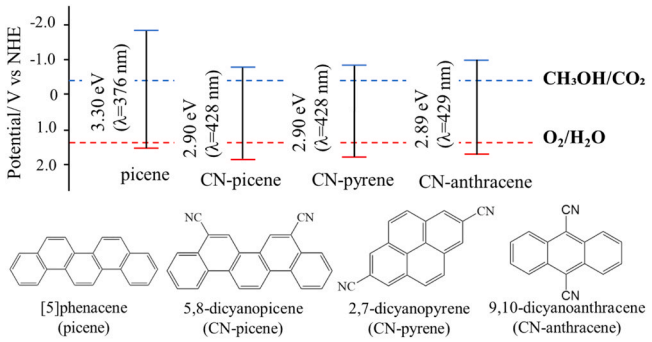

Fig. 1. HOMO–LUMO energy levels and gaps of organic photocatalysts calculated using DFT.

Table 1
Energy gap of various organic photocatalysts calculated using DFT.

Photocatalyst	HOMO (eV)	LUMO (eV)	Energy gap (eV)	Wavenumber (nm)
Picene	1.40	−1.90	3.30	328
CN-picene	1.96	−0.94	2.90	428
CN-pyrene	1.86	−1.04	2.90	428
CN-anthracene	1.76	−1.14	2.89	429

demonstrated that picene is an efficient photocatalyst for hydrogen generation via water splitting under UV irradiation [23]. In this study, the DFT-predicted energy levels of picene show that its HOMO energy level is more positive than the oxygen evolution potential (+1.23 eV vs NHE) associated with the oxidation of water, while the LUMO energy level is more negative than both the hydrogen evolution potential (0 eV vs NHE) for water reduction and the reduction potential for CO_2 to methanol (-0.38 eV vs NHE).

Therefore, the energy levels of the HOMO and LUMO in picene are not only suitable for hydrogen production via water splitting reactions but also for CO_2 reduction to methanol. To validate the DFT predictions, experiments were conducted using picene as a photocatalyst to investigate CO_2 reduction to methanol under UV and visible light. Fig. 2 shows that methanol is produced from picene when exposed to UV light; however, methanol production is not observed when exposed to visible light. Under UV light irradiation, H_2, O_2, and CO were also observed as byproducts by qualitative analysis. The results shown in Fig. 2 corroborate the DFT predictions, demonstrating that picene exhibits photocatalytic activity under UV light but not under visible light.

3.2. CO_2 reduction of several photocatalysts under visible light

The photocatalysts, picene, CN-picene, CN-pyrene, and CN-anthracene, were compared based on CO_2 reduction to methanol under visible light irradiation. Fig. 3 shows that methanol can be produced under visible light irradiation using CN-picene, CN-pyrene and CN-anthracene as photocatalysts, as DFT predictions. Among the tested photocatalysts, CN-anthracene can be observed to exhibit the highest methanol production activity (Fig. 3). DFT-calculated iso-surfaces of the excited state of CN-anthracene showed that CN-anthracene promoted charge separation (Figure S1).

Whereas, Table S1 shows the amount of hydrogen produced when CN-picene, CN-pyrene, and CN-anthracene are irradiated with visible light in the presence of CO_2 and H_2O. In contrast to the amount of methanol produced, CN-pyrene produced the most hydrogen, while CN-anthracene produced the least. It is generally known that the water decomposition reaction and the CO_2 reduction reaction proceed competitively. This indicates that even when using an organic photocatalyst, the hydrogen production reaction is suppressed when methanol production is dominant.

In CN-anthracene, the DFT-calculated spatial distribution of electron orbitals in the HOMO showed electron distribution over the entire molecule, whereas that in the LUMO indicated electron localization around the cyano groups. Thus, spatial localization of electrons in the HOMO and LUMO of CN-anthracene could be a key factor contributing to the efficient separation and transport of photogenerated charge, thereby suppressing recombination of holed and electrons. Hence, it is speculated that CN-anthracene has high activity in comparison with other organic photocatalysts. On the other hand, the electron distributions in the HOMO and LUMO of CN-pyrene were also calculated (Figure S2). The HOMO and LUMO in CN-pyrene, exhibited nearly identical electron distributions, suggesting that the photogenerated electrons were less likely to migrate and were more likely to recombine with the photogenerated holes. This difficulty in recombining electrons and holes may be the reason why the methanol production reaction by reduction of CO_2, which involves a more complex reaction pathway, proceeds preferentially in CN-anthracene.

3.3. Characterisation of CN-anthracene

The UV–vis absorption spectrum of CN-anthracene was measured. Fig. 4 shows that CN-anthracene exhibits an absorption peak at 2.9 eV (λ = 427 nm). The position of the absorption peak observed in the UV–vis spectrum of CN-anthracene is almost identical to the maximum absorption wavelength calculated from the HOMO-LUMO energy gap predicted by DFT. The photoluminescence (PL) spectrum of CN-anthracene was measured, and the results are presented in Fig. 5. The absorption near 440 nm, which is close to the maximum absorption wavelength (λ = 427 nm) calculated using DFT, can be detected alongside a fluorescence signal at approximately 530 nm. The signal in the PL spectrum of CN-anthracene can be ascribed to originate during the charge relaxation process, transitioning from LUMO of CN-

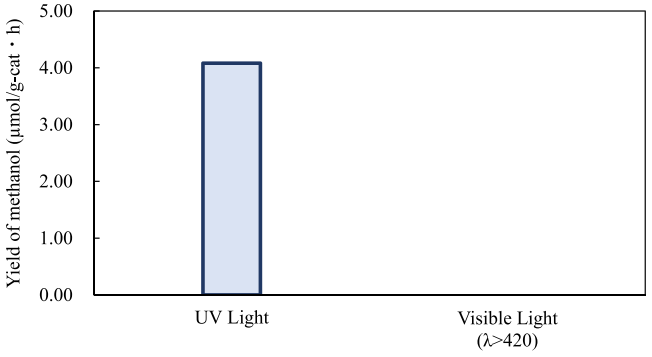

Fig. 2. Yield of methanol obtained via CO_2 reduction with H_2O using picene as a photocatalyst under UV or visible light irradiation.

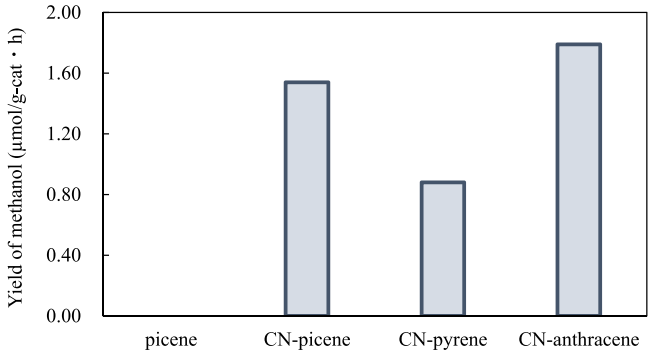

Fig. 3. Yield of methanol obtained via CO_2 reduction with H_2O using picene, CN-picene, CN-pyrene and CN-anthracene as photocatalysts under visible light irradiation (λ > 420 nm).

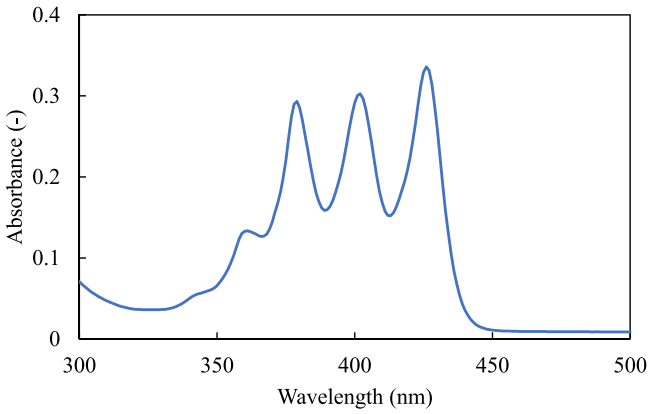

Fig. 4. UV–vis spectrum of CN-anthracene in toluene solution at room temperature (~298 K).

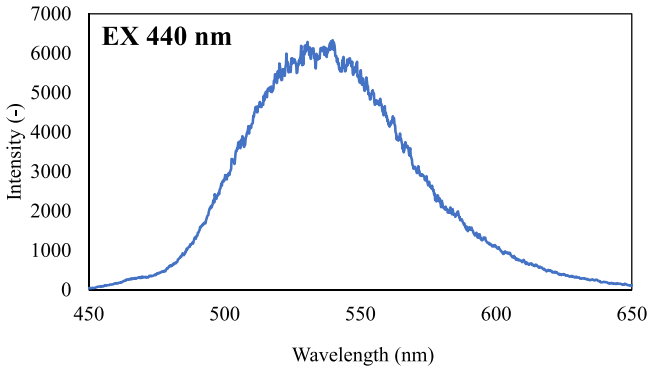

Fig. 5. PL spectrum of CN-anthracene obtained using an excitation wavelength of 440 nm.

anthracene to the HOMO. The results shown in Fig. 4 and 5 indicate that CN-anthracene exhibits absorption and emission at wavelengths nearly identical to those predicted using DFT. Hence, it is predicted that CN-anthracene has the ability to exhibit photocatalytic activity when exposed to visible light irradiation.

To examine the HOMO-LUMO levels of photocatalysts in more detail, this method of measuring the energy gap using PL spectra was applied to other catalysts. Table S2 shows the HOMO levels of photocatalysts considering the solvent effect of water, and the LUMO levels calculated from the energy gap measured by PL spectra. These results suggest that CN-picene, CN-pyrene, and CN-anthracene can reduce methanol under visible light irradiation.

3.4. Photocatalytic performance of CN-anthracene

Fig. 6 shows the time-dependent variation in methanol production during the CO_2 reduction reaction performed using CN-anthracene as a photocatalyst. In Fig. 6, methanol production can be observed to start at approximately 6 h after light irradiation, and the amount of methanol produced can be observed to have increased with irradiation time. Time profile of methanol yield in the early stage of irradiation is thought to be due to induction phase, catalyst activation, or some kinetic limitation. After 18 h of irradiation, the rate of methanol production decreases. The reduced methanol production rate is likely resulting from the use of batch-type reactor, where the excessive accumulation of methanol may inhibit further production.

Control experiments for the photocatalytic reaction using CN-anthracene were conducted. According to the data presented in Table 2, under conditions without a photocatalyst, light irradiation, or CO_2, no methanol production occurs. Methanol production occurs only

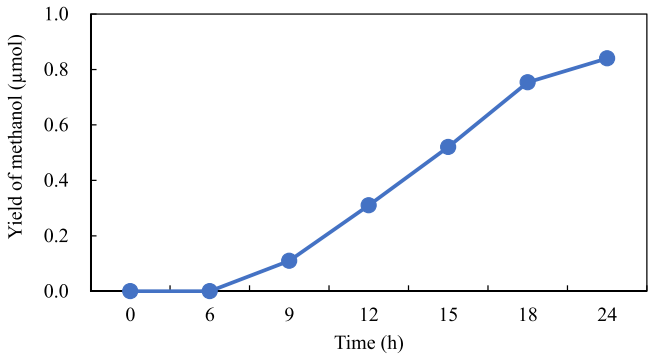

Fig. 6. Yield of methanol obtained via CO_2 reduction with H_2O using CN-anthracene under visible light irradiation ($\lambda > 420$ nm) as a function of irradiation time.

Table 2
Yield of methanol from CN-anthracene under different conditions. Irradiation time = 24.

Wavelength (nm)	Catalyst	Reactant	Yield of methanol (μmol)
> 420	-	CO_2	N.D.
-	CN-anthracene	CO_2	N.D.
> 420	CN-anthracene	-	Trace
> 420	CN-anthracene	CO_2	0.84

under conditions where a photocatalyst, light exposure, and CO_2 are all present. The results presented in Table 2 demonstrate that CN-anthracene can effectively function as a catalyst for the light-driven of CO_2 reduction.

The changes in methanol production during CO_2 reduction reactions performed using CN-anthracene as a photocatalyst under varying intensities of visible light were evaluated, and the results are shown in Fig. 7. Illuminance at 560 nm was measured using a light meter (CUSTOM LX-3000), and the irradiance was calculated. Fig. 7 shows that as the irradiance increases, methanol production also increases, suggesting that higher light intensity enhances the generation of electron-hole pairs in CN-anthracene, thereby promoting the CO_2 reduction reaction.

Fig. 8 presents the results of reusability tests performed on CN-anthracene as a photocatalyst. After each reaction under light irradiation, the CN-anthracene photocatalyst was recovered, washed with deionized water, vacuum-dried, and reused for subsequent photocatalytic reactions. After the third light irradiation cycle, the methanol production activity was observed to remain nearly identical to that observed during the first cycle, indicating that the structure of CN-anthracene remains relatively stable under light irradiation. It is

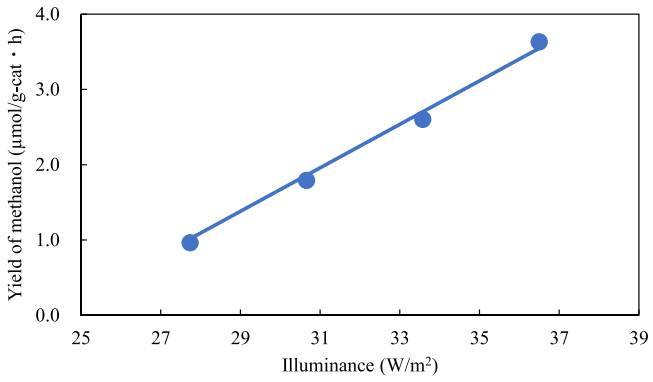

Fig. 7. Yield of methanol obtained via CO_2 reduction with H_2O using CN-anthracene under irradiation performed at different visible light intensities.

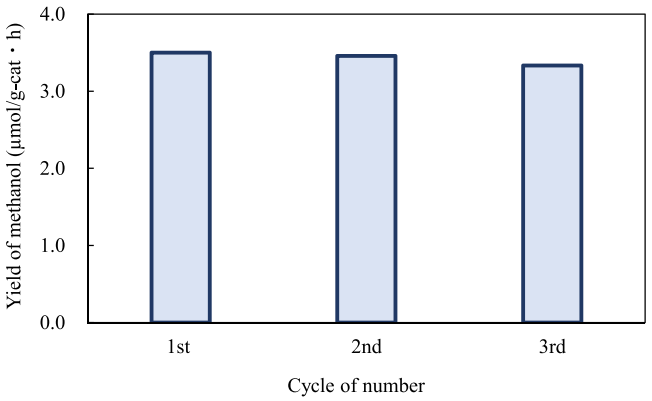

Fig. 8. Results of reusability tests showing yield of methanol obtained via CO_2 reduction with H_2O using CN-anthracene under visible light irradiation(λ > 420 nm).

obvious that CN-anthracene does not undergo significant structural changes during the CO_2 reduction reaction.

FT-IR spectra of CN-anthracene measured before and after light irradiation shows a distinct peak around 2220 cm^{-1}, corresponding to the cyano group (Figure S3) [30]. The intensity and position of the characteristic FT-IR of CN-anthracene remain unchanged before and after light irradiation, confirming that CN-anthracene retains its chemical structure under light irradiation, functioning effectively as a photocatalyst for CO_2 reduction.

3.5. Mass spectrometry of photocatalytic products obtained using CN-anthracene

Fig. 9(a) shows the mass spectrum of the products obtained via CO_2 reduction with H_2O using CN-anthracene as a photocatalyst, and a typical peak of methanol (CH_2OH^+: $m/z = 31$) can be observed. CH_3OH is also expected to appear at $m/z = 32$. However, due to the presence of trace amount of air in the measurement system, the peak detected at $m/z = 32$ corresponding to CH_3OH cannot be distinguished from that of atmospheric O_2 at $m/z = 32$. Fig. 9(b) shows the mass spectrum of the products obtained via CO_2 reduction with D_2O using CN-anthracene as a photocatalyst. In the products obtained using D_2O, instead of H_2O, for photocatalytic reduction of CO_2, deuterated methanol (CD_3OD) and its fragment ion (CD_2OD^+) are expected to occur at $m/z = 36$ and 34, respectively. Thus, Fig. 9(b) shows a characteristic peak at $m/z = 34$. In conclusion, it is indicated that the production of methanol via CO_2 reduction using CN-anthracene results from H_2O, without involving the decomposition of this photocatalyst.

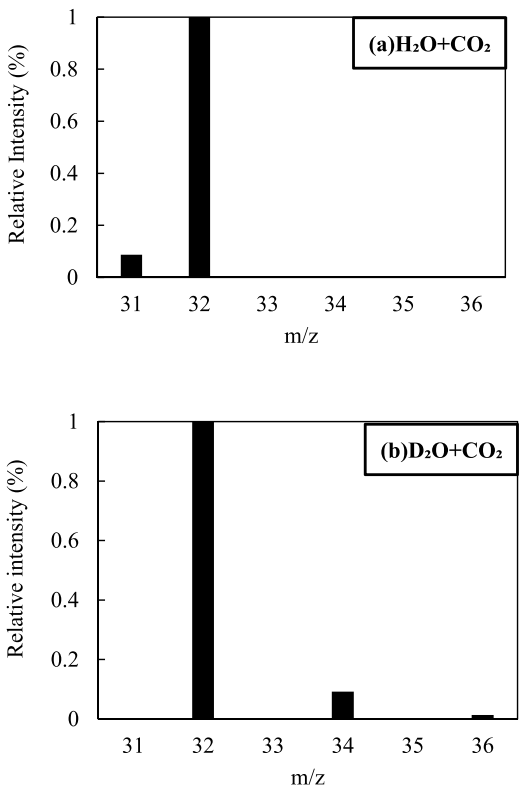

Fig. 9. Mass spectra of products obtained via photocatalytic reduction of CO_2 with (a) H_2O or (b) D_2O using CN-anthracene.

4. Conclusion

Methanol production via CO_2 reduction with water was successfully achieved using CN-anthracene, selected as a photocatalyst through DFT calculations. Computational science based on DFT calculations is highly effective in predicting the potential of photocatalysts to facilitate CO_2 reduction. Reusability experiments showed that the methanol production performance of CN-anthracene does not decrease even after repeated use. Experimental results demonstrated that CN-anthracene, exhibiting a relatively stable structure, can be effectively utilized for CO_2 reduction through photocatalytic processes. The mass spectrometry results further confirmed that the produced methanol utilizes water and carbon dioxide as reactants, without involving the decomposition of the photocatalyst. The reduction reaction of CO_2 using organic photocatalysts proceeds through competitive reactions with water decomposition reactions, making it difficult to discuss solely in terms of energy gaps. Since the reaction that produces the methanol has the complex elementary reactions, it is necessary to examine the reaction mechanism in greater detail and discuss it using kinetic theory and energy theory. However, in this study, it was demonstrated that the molecular catalyst, organic photocatalyst, provides a rough guideline for whether the reaction can proceed based on the calculation of the HOMO-LUMO energy gap. It is expected that this will be helpful for future catalyst development.

CRediT authorship contribution statement

Daisuke Nishikawa: Methodology. **Kazuki Shishida:** Writing – original draft, Methodology, Investigation. **Kaito Oishi:** Investigation. **Yuichi Ichihashi:** Writing – review & editing, Supervision, Methodology, Conceptualization.

Funding

This research did not receive any specific grant from funding agencies in the public, commercial, or not-for-profit sectors.

Declaration of Competing Interest

The authors declare that they have no known competing financial interests or personal relationships that could have appeared to influence the work reported in this paper.

Acknowledgements

We would like to thank Editage (www.editage.jp) for English language editing.

Appendix A. Supporting information

Supplementary data associated with this article can be found in the online version at doi:10.1016/j.cattod.2025.115530

Data Availability

No data was used for the research described in the article.

References

[1] Y. Liu, L. Liu, M. Irfan, T.S. Adebayo, M. Das, K. Khudoykulov, A safe path towards carbon neutrality by 2050: assessing the impact of oil and gas efficiency using advanced quantile-based approaches, J. Clean. Prod. 425 (2023) 138844, https://doi.org/10.1016/j.jclepro.2023.138844.

[2] É. Yáñez, H. Meerman, A. Ramírez, É. Castillo, A. Faaij, Assessing bio-oil co-processing routes as CO_2 mitigation strategies in oil refineries mitigation strategies in oil refineries, Biofuels Bioprod. Biorefin. 15 (2021) 305–333, https://doi.org/10.1002/bbb.2163.

[3] S.N. Habisreutinger, L. Schmidt-Mende, J.K. Stolarczyk, Photocatalytic reduction of CO_2 on TiO_2 and other semiconductors$_2$ on TiO_2 and other semiconductors, Angew. Chem. Int. Ed. 52 (2013) 7372–7408, https://doi.org/10.1002/anie.201207199.

[4] Y. Horiuchi, K. Miyazaki, M. Tachibana, K. Nishigaki, M. Matsuoka, Solar light-driven selective photoelectrochemical CO_2 reduction to CO in aqueous media using si nanowire arrays decorated with au and Au-based metal nanoparticles, Res Chem. Inter. 49 (2023) 1131–1146, https://doi.org/10.1007/s11164-023-04959-y.

[5] J. Ran, M. Jaroniec, S.Z. Qiao, Cocatalysts in semiconductor-based photocatalytic CO_2 reduction: achievements, challenges, and opportunities$_2$ reduction: achievements, Adv. Mater. 30 (2018) 1704649, https://doi.org/10.1002/adma.201704649.

[6] W. Tu, Y. Zhou, Z. Zou, Photocatalytic conversion of CO_2 into renewable hydrocarbon fuels: State-of-the-art accomplishment, challenges, and prospects, Adv. Mater. 26 (2014) 4607–4626, https://doi.org/10.1002/adma.201400087.

[7] W. Dai, H. Xu, J. Yu, X. Hu, X. Luo, X. Tu, L. Yang, Photocatalytic reduction of CO_2 into methanol and ethanol over conducting polymers modified Bi_2WO_6 microspheres under visible light, Appl. Surf. Sci. 356 (2015) 173–180, https://doi.org/10.1016/j.apsusc.2015.08.059.

[8] U.I. Gaya, A.H. Abdullah, Heterogeneous photocatalytic degradation of organic contaminants over titanium dioxide: a review of fundamentals, progress and problems, J. Photochem. Photobiol. C. Photochem. Rev. 9 (2008) 1–12, https://doi.org/10.1016/j.jphotochemrev.2007.12.003.

[9] S. Ijaz, M.F. Ehsan, M.N. Ashiq, N. Karamat, T. He, Preparation of CdS@CeO_2 core/shell composite for photocatalytic reduction of CO_2 under visible-light irradiation, Appl. Surf. Sci. 390 (2016) 550–559, https://doi.org/10.1016/j.apsusc.2016.08.098.

[10] N. Kitjanukit, W. Neamsung, A. Karawek, N. Lertthanaphol, N. Chongkol, K. Hiramatsu, T. Sekiguchi, S. Pornsuwan, T. Sakurai, W. Jonglertjunya, P. Phadungbut, Y. Ichihashi, S. Srinives, Effects of alcohols as sacrificial reagents on a copper-doped sodium dititanate nanosheets/graphene oxide photocatalyst in CO_2 photoreduction photoreduction, RSC Adv. 14 (2024) 27980–27989, https://doi.org/10.1039/D4RA04585H.

[11] Y. Xu, J. Yu, J. Long, L. Tu, W. Dai, L. Yangm, Z-Scheme heterojunction of SnS_2/Bi_2WO_6 for photoreduction of CO_2 to 100% alcohol products by promoting the separation of photogenerated charges, Nanomaterials 12 (2022) 2030, https://doi.org/10.3390/nano12122030.

[12] H. Abdullah, M.M.R. Khan, H.R. Ong, Z. Yaakob, Modified TiO_2 photocatalyst for CO_2 photocatalytic reduction: an overview, J. CO2 Util. 22 (2017) 15–32, https://doi.org/10.1016/j.jcou.2017.08.004.

[13] E. Karamian, S. Sharifnia, On the general mechanism of photocatalytic reduction of CO_2, J. CO2 Util. 16 (2016) 194–203, https://doi.org/10.1016/j.jcou.2016.07.004.

[14] D. Luo, C. Chen, N. Zhang, S. Hong, H. Wu, Z. Liu, Characterization and DFT research of Nd/TiO_2: photocatalyst for synthesis of methanol from CO_2 and H_2O, Z. Phys. Chem. 223 (12) (2010), https://doi.org/10.1524/zpch.2009.5497.

[15] F. Solymosi, I. Tombácz, Photocatalytic reaction of H_2O + CO_2 over pure and doped Rh/TiO_2, Catal. Lett. 27 (1994) 61–65, https://doi.org/10.1007/BF00806978.

[16] S. Zhang, X. Yin, Y. Zheng, Enhanced photocatalytic reduction of CO_2 to methanol by ZnO nanoparticles deposited on ZnSe nanosheet, Chem. Phys. Lett. 693 (2018) 170–175, https://doi.org/10.1016/j.cplett.2018.01.018.

[17] G. Gelinck, P. Heremans, K. Nomoto, T.D. Anthopoulos, Organic transistors in optical displays and microelectronic applications, Adv. Mater. 22 (2010) 3778–3798, https://doi.org/10.1002/adma.200903559.

[18] S. Naserian, M. Izadyar, E. Ranjbakhsh, Theoretical design of Au–DPPh–Au molecular junction for use in organic field-effect transistors, J. Phys. Chem. Solids 180 (2023) 111440, https://doi.org/10.1016/j.jpcs.2023.111440.

[19] A.F. Paterson, S. Singh, K.J. Fallon, T. Hodsden, Y. Han, B.C. Schroeder, H. Bronstein, M. Heeney, I. McCulloch, T.D. Anthopoulos, Recent progress in high-mobility organic transistors: a reality check, Adv. Mater. 30 (2018) 1801079, https://doi.org/10.1002/adma.201801079.

[20] Cui, Y. Fu, J. Song, B. Meng, J. Zhou, Z. Zhou, Z. Su, A Cu^I cluster-based covalent metal-organic framework as a photocatalyst for efficient visible-light-driven reduction of CO_2, ChemSusChem 16 (2023) e202202079, https://doi.org/10.1002/cssc.202202079.

[21] H. Sun, A. Putta, M. Billion, Arene trifluoromethylation: an effective strategy to obtain air-stable n-type organic semiconductors with tunable optoelectronic and electron transfer properties, J. Phys. Chem. A. 116 (2012) 8015–8022, https://doi.org/10.1021/jp301718j.

[22] D.D. Méndez-Hernández, P. Tarakeshwar, D. Gust, T.A. Moore, A.L. Moore, V. Mujica, Simple and accurate correlation of experimental redox potentials and DFT-calculated HOMO/LUMO energies of polycyclic aromatic hydrocarbons, J. Mol. Model 19 (2013) 2845–2848, https://doi.org/10.1007/s00894-012-1694-7.

[23] A. Okemoto, K. Kishishita, S. Maeda, S. Gohda, M. Misaki, Y. Koshiba, K. Ishida, T. Horie, K. Taniya, Y. Ichihashi, S. Nishiyama, Application of picene thin-film semiconductor as a photocatalyst for photocatalytic hydrogen formation from water, Appl. Catal. B. 192 (2016) 88–92, https://doi.org/10.1016/j.apcatb.2016.03.028.

[24] Y. Ichihashi, T. Sekiguchi, Y. Tokui, R. Hori, S. Naito, Y. Koshiba, Y. Sutani, K. Ishida, K. Taniya, S. Nishiyama, Decomposition of water over picene derivatives photocatalyst under visible light irradiation, Catal. Today 410 (2023) 317–322, https://doi.org/10.1016/j.cattod.2022.06.008.

[25] P.K. Kushwaha, D.K. Shatapathy, V. Sharma, S.K. Srivastava, Tuning optical and electronic properties of indanthrene derivatives with electron-withdrawing groups (–Cl, $–NO_2$ and –C≡N) for enhanced organic solar cell performance: a DFT approach, Phys. Scr. 100 (2025) 025907, https://doi.org/10.1088/1402-4896/ada0f3.

[26] E.T.L. Fei, J. Biswas, B. Datta, D. Kumar, Computational studies of diindole-based molecules for organic bulk heterojunction solar devices using DFT and TD-DFT calculations, Struct. Chem. 32 (2021) 1973–1984, https://doi.org/10.1007/s11224-021-01777-z.

[27] H. Okamoto, H. Takahashi, T. Takane, Y. Nishiyama, K. Kakiuchi, S. Gohda, M. Yamaji, Convenient phenacene synthesis by sequentially performed wittig reaction and mallory photocyclization using continuous-flow techniques, Synthesis 49 (2017) 2949–2957, https://doi.org/10.1055/s-0036-1588775.

[28] H. Okamoto, M. Yamaji, S. Gohda, Y. Kubozono, N. Komura, K. Sato, H. Sugino, K. Satake, Facile synthesis of picene from 1,2-di(1-naphthyl)ethane by 9-fluorenone-sensitized photolysis, Org. Lett. 13 (2011) 2758–2761, https://doi.org/10.1021/ol200874q.

[29] D. Zych, A. Slodek, Pyrene derivatives with two types of substituents at positions 1, 3, 6, and 8 – fad or necessity? RSC Adv. 9 (2019) 24015, https://doi.org/10.1039/C9RA04503A.

[30] X.L. Zhang, R.K. Gilpin, FT-IR studies of N-(p-Cyanobenzylidene)-p-octyloxyaniline, 4′-cyanobenzylidene-4-n-hexyloxyaniline and 4′-n-hexyloxybenlidene-4-cyanoaniline, Mol. Cryst. Liq. Cryst. 231 (1993) 57–68, https://doi.org/10.1080/10587259308032492.